

See discussions, stats, and author profiles for this publication at: <https://www.researchgate.net/publication/261746859>

Atomic-Layer Electroless Deposition: A Scalable Approach to Surface-Modified Metal Powders

ARTICLE *in* LANGMUIR · APRIL 2014

Impact Factor: 4.46 · DOI: 10.1021/la500477s · Source: PubMed

CITATION

1

READS

23

7 AUTHORS, INCLUDING:



[Patrick Cappillino](#)

University of Massachusetts Dartmouth

21 PUBLICATIONS 90 CITATIONS

[SEE PROFILE](#)



[Josh Sugar](#)

Sandia National Laboratories

33 PUBLICATIONS 314 CITATIONS

[SEE PROFILE](#)



[Zhi Liu](#)

ShanghaiTech University

189 PUBLICATIONS 3,200 CITATIONS

[SEE PROFILE](#)



[John L. Stickney](#)

University of Georgia

174 PUBLICATIONS 3,337 CITATIONS

[SEE PROFILE](#)

Atomic-Layer Electroless Deposition: A Scalable Approach to Surface-Modified Metal Powders

Patrick J. Cappillino,[†] Joshua D. Sugar,[†] Farid El Gabaly,[†] Trevor Y. Cai,[†] Zhi Liu,[‡] John L. Stickney,[§] and David B. Robinson^{†,*}

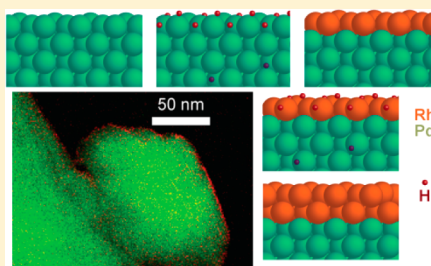
[†]Sandia National Laboratories, Livermore, California, United States

[‡]Advanced Light Source, Lawrence Berkeley National Laboratory, Berkeley, California, United States

[§]Department of Chemistry, The University of Georgia, Athens, Georgia, United States

Supporting Information

ABSTRACT: Palladium has a number of important applications in energy and catalysis in which there is evidence that surface modification leads to enhanced properties. A strategy for preparing such materials is needed that combines the properties of (i) scalability (especially on high-surface-area substrates, e.g. powders); (ii) uniform deposition, even on substrates with complex, three-dimensional features; and (iii) low-temperature processing conditions that preserve nanopores and other nanostructures. Presented herein is a method that exhibits these properties and makes use of benign reagents without the use of specialized equipment. By exposing Pd powder to dilute hydrogen in nitrogen gas, sacrificial surface PdH is formed along with a controlled amount of dilute interstitial hydride. The lattice expansion that occurs in Pd under higher H₂ partial pressures is avoided. Once the flow of reagent gas is terminated, addition of metal salts facilitates controlled, electroless deposition of an overlayer of subnanometer thickness. This process can be cycled to create thicker layers. The approach is carried out under ambient processing conditions, which is an advantage over some forms of atomic layer deposition. The hydride-mediated reaction is electroless in that it has no need for connection to an external source of electrical current and is thus amenable to deposition on high-surface-area substrates having rich, nanoscale topography as well as on insulator-supported catalyst particles. STEM-EDS measurements show that conformal Rh and Pt surface layers can be formed on Pd powder with this method. A growth model based on energy-resolved XPS depth profiling of Rh-modified Pd powder is in general agreement. After two cycles, deposits are consistent with 70–80% coverage and a surface layer with a thickness from 4 to 8 Å.



INTRODUCTION

Palladium has a wide variety of applications that include hydrogen storage and sensing,^{1–3} chemical catalysis,^{4–6} and fuel cell catalysis.^{7–9} In each of these areas, formation of atomic-scale surface and subsurface layers of other metals has been identified as a promising avenue for enhancement of properties.^{10–13} In the case of hydrogen storage and sensing, computational investigations suggest that such surface and near-surface layers have surface hydride energetics that differ from those of Pd, and this may enhance the kinetics of hydrogen absorption and desorption.¹² It has also been demonstrated that the catalytic properties of noble metals are sensitive to an overlayer of a metal in several important industrial reactions, including electro-oxidation of formic acid,^{14,15} oxygen reduction,¹⁶ and alcohol oxidation.¹⁷ In addition, the element present at the surface affects catalyst inactivation by poisons.¹⁸

In recent decades, several strategies for atomic layer deposition (ALD) have been reported in attempts to prepare materials such as those described above.¹⁹ In these techniques, self-limiting reactions are sequentially carried out at the surface of a material, creating a binary or multilayer film. These

processes are usually performed in the gas phase and at low pressure. Advantages include precise thickness control, based on the number of cycles performed, and the ability to deposit on high-aspect-ratio substrates. It has been recognized, however, that the high temperatures required for ALD of metals such as Pt (200–300 °C) are unsuitable for temperature-sensitive substrates.^{20,21} For example, nanopores in Pd and Pt display significant restructuring at temperatures above 200 °C, well below the melting points of the metals.^{22,23} The low temperatures to which these materials are limited to preserve nanostructure are insufficient to volatilize precursors or to remove ligands on adsorbed precursors, blocking subsequent cycles of conventional ALD.²⁴ To mitigate this problem, room-temperature ALD of Pt has recently been reported, in which an O₂ plasma was used to assist in ligand decomposition.²¹ Although this strategy was demonstrated to be effective for deposition of films, nanoporous substrates or those with complex surface topology, in which the access of the

Received: February 5, 2014

Revised: March 17, 2014

Published: April 4, 2014

plasma to some surface sites could be blocked, would present difficulties.

A solution-phase process known as electrochemical atomic layer deposition (E-ALD) has also been utilized for the formation of nanofilms on a variety of substrates.²⁵ This process is carried out under ambient conditions, in condensed phases, and allows conformal deposition with tunable thickness. Despite these advantages, deposition is confined to the surface of an electrode that must be in electrical contact with an external instrument. The amount of current supplied by the instrument and also by a counter electrode scales with the surface area of the substrate. This is problematic in the case of metal structures with high surface areas, such as nanoporous metals, fine powders, and catalysts supported on insulating substrates, such as silica or alumina.

In the approach presented here, layer-by-layer deposition of elements more noble than PdH was carried out by charging Pd powders with a controlled partial pressure of H₂ gas to chemically form a surface hydride. After terminating the flow of reagent gas, the hydride was used for controlled reduction of an adlayer of a different metal at the surface of the particles, with repetition of these two steps as needed to obtain a desired thickness (Scheme 1). This approach has many of the same

deposition (UPD) layer (typically Cu or Pb) of atomic thickness is formed electrochemically and then replaced by a more noble metal. These steps are repeated to form thicker films.^{27–30} SLRR using hydrogen UPD to deposit Pt was recently reported as the first example of this technique with a nonmetal sacrificial layer.³¹

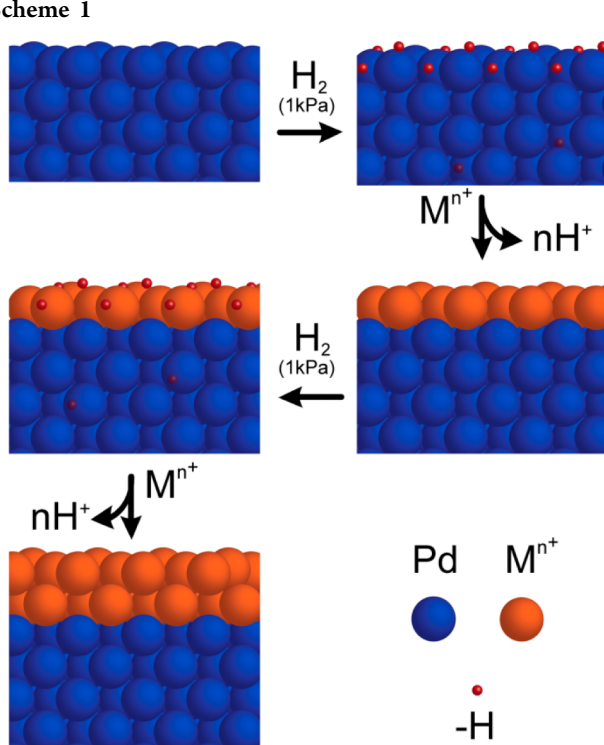
The lattice-expanded, β -phase PdH (PdH_{β}) has a H/Pd ratio in the bulk of the material of ~ 0.65 , and the hydride species are mobile enough to react at the surface. Formation of PdH_{β} either electrochemically³² or by exposure to pure H₂,³³ followed by galvanic replacement of the hydride with metal salts, has been previously reported. The latter reference bears a procedural resemblance to the work described here; however, such reactions are far from being surface-limited. Except in films a few nanometers thick, the amount of hydride in the bulk is much greater than the amount on the surface. This reaction has been shown to form dendrites rather than a conformal layer.³² Such dendritic growth has been prevented in the present case by limiting the H₂ partial pressure, avoiding formation of PdH_{β} . In the more dilute α -phase PdH (PdH_{α}), the amount of bulk hydride is much lower and can be controlled so that it is comparable to or less than the amount of surface hydride. The reaction is thus essentially surface-limited. Such conditions allow formation of a conformal overlayer having a thickness from one to a few monolayers.

Reductive deposition of very dilute salts of Pd and Rh as atomic-scale films on single crystal Pt by exposure to H₂/Ar gas mixtures has been demonstrated previously.^{34,35} In the present work, this general strategy is modified for large-scale application to polycrystalline powders with much greater surface area and more robust control of thickness. Further, in the case of hydrogen absorbing substrates such as Pd, the controlled partial pressure of H₂ gas, demonstrated herein, is necessary for the reasons discussed above. The cyclic exposure of substrate to reagent gas, followed by doses of metal salt under static pressure, is a more effective means of large-scale conformal deposition of many adlayers and precludes formation of nanoparticles (NP).

Herein, we demonstrate a means of atomic-layer electroless deposition (ALED) of Rh and Pt metal on Pd powder (PdPt, PdRh). This process is carried out by suspending the powder in an electrolyte solution and cycling between chemical hydride formation using dilute hydrogen gas in nitrogen and addition of salts of the metals to be deposited. As the number of cycles increases, the thickness of the surface layer increases, as shown by X-ray photoelectron spectroscopy (XPS). Changes to the cyclic voltammetry (CV) of PdPt and PdRh powders demonstrate kinetic enhancement of hydrogen desorption after formation of the adlayer, as has been observed in the case of nanofilms.^{13,36} A growth model is presented that is based on energy-resolved X-ray photoelectron spectroscopy (ERXPS), is consistent with high-resolution scanning transmission electron microscopy (STEM) measurements, and suggests a conformal layer forms during the course of ALED. Some three-dimensional growth is indicated, but large-scale island and dendrite formation does not occur. To establish relevance to applications that involve supported catalysts, we also demonstrate that this technique can be carried out on commercially obtained palladium on carbon (Pd/C).

EXPERIMENTAL SECTION

Materials. The palladium powder used in this study was obtained from Engelhard. Rhodium(III) chloride, ammonium



advantages as the electroless process known as successive ionic layer adsorption and reaction.²⁶ In that technique, metal chalcogenide thin films are deposited using controlled formation and precipitation of adlayers of ions. Advantages of this process include ambient operating conditions that are amenable to temperature-sensitive substrates, scalability to large amounts of high-surface-area materials, and tolerance to polycrystalline substrates with rough surfaces that would be useful on an industrial scale.

The strategy presented herein also bears similarity to an implementation of E-ALD known as surface-limited redox replacement (SLRR), in which a sacrificial, underpotential

tetrachloropalladate, and Pt wire were purchased from Alfa Aesar. Ammonium tetrachloroplattinate was obtained from City Chemicals. Reagent gas (1% hydrogen, 99% nitrogen) was obtained from Matheson Tri-Gas. Pd wire was obtained from Sigma-Aldrich. Pd/C (10% Pd) was obtained from Strem Chemicals.

Physical Methods. All electrochemistry was carried out using a Bio-Logic SP-200 potentiostat. Open-circuit potential (OCP) experiments were carried out by monitoring the potential of the Pd working electrode (WE) over time, with no applied current or potential, during ALED cycles. Ag/AgCl reference (3.5 M KCl) and Pt wire (0.5 mm diameter) counter electrodes were used to measure the CV of the Pd wire (0.25 mm diameter), with 0.1 M sulfuric acid electrolyte and a scan rate of 150 mV/s. To measure the CV of the ALED samples subsequent to deposition, a working electrode was made by pressing a known quantity of powder into a flat cake on a piece of gold-coated silicon wafer. The sample was covered with a porous polypropylene membrane (Celgard 3501) and assembled into a “plate material evaluating cell” (BASi) with Ag/AgCl reference (3.5 M KCl) and Pt wire (0.5 mm diameter) counter electrodes and 0.1 M sulfuric acid electrolyte. Measurements were performed with the cell under N₂ purge.

XPS experiments on powder samples were conducted using an Al K α source (Omicron model DAR400) using photons of 1490 eV. Photoelectrons with kinetic energies between 1127 and 1490 eV were detected using a Physical Electronics model 10-360 electron energy analyzer. At this photon energy, the photoelectrons from the 3d orbitals of Pd and Rh have mean free paths (MFPs) of 2.0 and 1.6 nm, respectively, and those from the 4f orbitals of Pt have a MFP of 1.7 nm.³⁷ The powder samples were pressed into an alloy foil (Pb_{92.5}Sn₃Ag_{2.5}) obtained from Indium Corporation for mounting. Prior to analysis, samples were exposed to H₂ gas (7 Pa) at room temperature to remove surface oxide that had formed adventitiously during sample preparation and storage.

Further XPS experiments on these samples using varied incident photon energies for depth-profile experiments were conducted at the Advanced Light Source at Lawrence Berkeley National Laboratory (XPS endstation at beamline 9.3.2).³⁸ Spectra were collected at X-ray photon energies of 450 and 850 eV. The resultant photoelectrons from the 3d orbitals of Pd and Rh have MFPs of 0.5 and 0.4 nm, respectively, at 450 eV and 1.1 and 0.9 nm, respectively, at 850 eV.³⁷ Photoelectrons originating from the Pt 4f orbitals have MFPs of 0.7 and 1.1 nm using 450 and 850 eV X-ray photons, respectively.³⁷ The software program SESSA (Simulation of Electron Spectra for Surface Analysis) was used to simulate spectra at the three incident photon energies used in the XPS experiments.³⁹ Integration of experimental and simulated spectra was carried out with the software program CasaXPS after background correction, using the scaling factors included with the program.

BET surface area measurements of the Pd starting material were made using a Micromeritics ASAP 2020 porosimeter. Nitrogen gas at 77 K was used as the adsorptive, and samples were degassed for 15 h at 50 °C prior to analysis.

Scanning electron microscopy (SEM) was carried out using a JEOL JSM 7600F field-emission electron microscope with the powder samples embedded in carbon paint.

Ultraviolet-visible spectroscopy was carried out on a Shimadzu UV-3600 UV-vis-NIR spectrometer.

PdRh powder particles were sectioned in accordance with literature procedures^{40,41} so that the compositional distribution of Rh could be imaged with STEM. The powder was encapsulated in an epoxy formulation that cured at room temperature (Struers). The epoxy was then sectioned with a diamond knife at room temperature using a Leica EM UC6 ultramicrotome. The resulting samples were electron-transparent and suitable for compositional analysis, which was performed using a probe-corrected FEI Titan G2 80-200 with a large-area silicon drift EDS detector (ChemiSTEM). EDS spectrum images were acquired with an EDS spectrum at every image pixel. Quantitative compositional analysis was performed using the Cliff-Lorimer *k* factor method.⁴² Spectral reference shapes for Pd and Rh were measured from pure materials and used in multiple least-squares fits of background-subtracted spectra of unknown composition. The *k* factor was measured from a known reference material (8 at. % Rh–Pd), whose composition was verified by calibrated X-ray fluorescence measurements.

Preparation of Surface-Modified Powders. For deposition experiments, a 3-neck flask (100 mL) was used, with a gas inlet capable of bubbling either N₂ gas or reagent gas (1% H₂ in N₂) through the electrolyte. The flask also contained reference, counter, and working electrodes, and a stir bar. A schematic of the cell used is shown in Figure S1 of the Supporting Information. Prior to use, the WE was laminated with polypropylene, exposing 2 cm, to ensure that a consistent surface area was in contact with the electrolyte solution before and after deposition experiments. The cell was filled with 30 mL of 0.1 M H₂SO₄ that was purged with N₂ gas prior to the initial CV. The cell was then charged with a known quantity of Pd powder (250 to 300 mg), and the gas flow was switched to the reagent gas. The OCP was then monitored with time until it stabilized (~−0.2 V vs Ag/AgCl). The reagent gas bubbling was then discontinued, leaving the cell under static pressure, and N₂-purged RhCl₃ or (NH₄)₂(PtCl₄) salts (~10 mM in 0.1 M H₂SO₄) were added by syringe to prepare PdRh and PdPt. Aliquots (0.1 to 1.0 mL) containing from 0.36 to 44 mmol metal salt per mol Pd were used in various deposition experiments. This procedure of purging under reagent gas until a stable OCP was reached, followed by addition of metal salt aliquots, was repeated for up to eight cycles. After deposition, the modified powder was removed from the cell, filtered, rinsed several times with deionized water, and dried overnight at room temperature under reduced pressure. A sample of PdPd was prepared for control experiments by addition of 4.8 mmol (NH₄)₂(PdCl₄) per mol Pd powder using the above procedure. A sample of PdRh in which Pd/C was used as a substrate was prepared in a similar manner, with an aliquot (2.0 mL, 50 mM) of RhCl₃ added to the suspended, finely divided powder (250 mg, 0.24 mmol Pd) in one cycle of ALED.

RESULTS AND DISCUSSION

ALED of Pt and Rh on Pd Powder. Exposure of a suspension of Pd powder in electrolyte to hydrogen/nitrogen gas mixtures should have the following consequences: (i) reduction of oxide present at the surface of the Pd particles,⁴³ (ii) formation of a surface hydride due to the large enthalpy of chemisorption of hydrogen on Pd,⁴⁴ and (iii) formation of dilute, bulk, α -phase palladium hydride (PdH_{*a*}).⁴⁵ By controlling the partial pressure of H₂ in the gas mixture, this third step can be precisely tuned, given that the stoichiometry

of PdH_α as a function of H_2 partial pressure is well known.⁴⁵ Notably, at 30 °C, the maximum solubility of PdH_α is 0.015 H/Pd, and this value is reached at 2.4 kPa of H_2 pressure.⁴⁶ Above this pressure, PdH_α is converted to PdH_β , so this represents an upper limit on the H_2 pressure to be used at this temperature. Under these temperature and partial pressure conditions, when considering films and fine powders, the equilibrium amount of hydride in the bulk is less than or similar to the amount on the surface. Electroless deposition of metals can then be carried out by exposing the hydrided substrate to the corresponding metal ions in solution.

The partial pressure of hydrogen gas is an important factor in controlling the amount of bulk PdH_α formed during charging. The surface area of the Pd powder used in these investigations was measured to be $1.0 \text{ m}^2 \text{ g}^{-1}$, so we expect from 2.6 to 2.3 mmol of surface atoms per mol Pd. These upper and lower bounds for the polycrystalline powder are estimated using the number of atoms in a unit area of (111) and (100) fcc Pd (assuming a lattice parameter of 3.89 Å), along with the surface area of the powder and the atomic mass of Pd.⁴⁶ For the purposes of identifying experimental samples discussed here, we define a dose unit (DU) as consisting of 2.6 mmol metal salt per mol Pd. Upon exposure of this Pd powder to a partial pressure of 1.0 kPa H_2 , PdH_α should form and dissolve in the Pd at a ratio of $\sim 8.5 \times 10^{-3}$ H/Pd, which is from 3.3 to 3.7 surface equivalents based on the upper and lower bounds calculated above.⁴⁵ Further, even at extremely low H_2 pressure, a surface hydride would form and provide an additional reducing equivalent for surface deposition.⁴⁴

Using Rh as an example, since deposition of a single monolayer (ML) of atoms at the surface of Pd metal by reduction of Rh^{3+} ions requires 3 equiv of PdH , each cycle of hydride formation under these conditions would provide reducing equivalents necessary for deposition of 1.3 to 1.7 ML. Solution-phase hydrogen does not contribute significantly to the number of reducing equivalents, especially since the reagent gas bubbling is stopped, and the cell is under static pressure during deposition of the metal salt. The solubility of H_2 in the aqueous phase is on the order of 10 μM at a gas partial pressure of 1 kPa, so approximately 0.3 μmol is dissolved in the aqueous phase.⁴⁷ This is small compared with the ~5 μmol of Pd surface atoms present. A few tens of micromoles of H_2 are also present in the headspace, but evidence suggests that this gas does not reduce the metal salt on the experimental time scale. It is left in the vessel in an attempt to keep hydrogen near equilibrium among all phases present, although it would be sensible to reduce the headspace volume in future designs. The partial pressure used in this example is close to the upper limit that is advisable when using a Pd substrate at room temperature. Powder exposed to >1.6 kPa of H_2 at 22 °C would undergo transformation to PdH_β , with a corresponding increase in volume, leading to formation of undesirable dendrites rather than a conformal surface layer.^{32,48}

In contrast to conventional ALD, in which adlayer growth is limited to the surface by the adsorption of the precursor, in the present case, two important conditions are necessary to control adlayer growth. First, by using a low partial pressure of H_2 and keeping the cell under static pressure during the deposition phase of each cycle, the reducing agent present is limited to surface hydride and dilute PdH_α that can migrate to the surface. Second, for many cycles of deposition, the dose of metal salt should be limited to the amount of reducing agent present from the hydride forming phase. A presence of excess metal salt in

solution during subsequent hydride forming phases may affect growth. A strategy to mitigate this in future implementations would be to make use of a flow cell to introduce the metal salt in a controlled fashion and remove excess metal salt between cycles.^{28,36}

The polycrystalline Pd substrate particles before and after ALED of Rh are shown in SEM micrographs in Figure 1. The aggregated spheroids had diameters ranging from several hundred nanometers to 1 μm. At this scale, the particles exhibited no changes due to the deposition process.

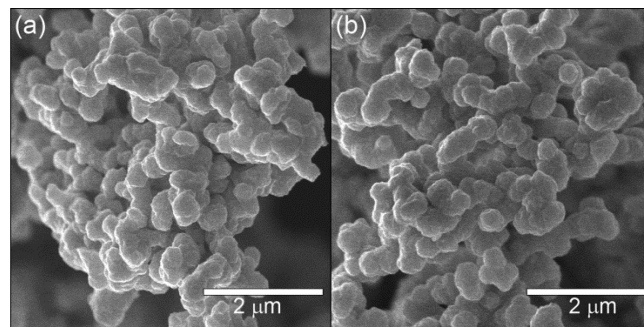


Figure 1. SEM images of Pd powder used as the substrate for ALED, before (a) and after (b) Rh deposition.

As the Pd particles, suspended in electrolyte, were exposed to 1% H_2/N_2 gas, the OCP between the Pd working and Ag/AgCl reference electrodes immersed in the reaction cell was measured (Figure 2). An immediate, steep drop in potential

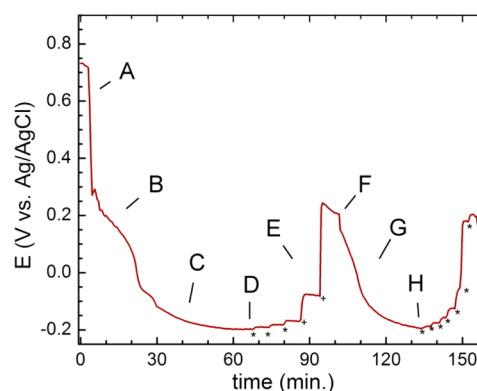


Figure 2. Change in open-circuit potential over time (regions A–H) as Pd powder suspended in H_2SO_4 (0.1M) is alternately exposed to 1% H_2/N_2 gas and aliquots of RhCl_3 (12.8 mM) with volumes of 0.10 mL (*) and 0.25 mL (+).

was observed due to changes at the surface of the Pd WE (region A, Figure 2). The OCP decreased more slowly from ~0.3 to ~0.1 V (region B, Figure 2). The shallower slope in region B is likely due to the gradual reduction of an oxide layer on the powder particles. This potential range is slightly below the observed surface oxide reduction peak in the CV of the bare Pd wire taken prior to experiments, at ~0.4 V. In the absence of stirring, we have observed that the OCP decreases much more quickly and then increases back to the range of region B. With stirring, the presence of oxide on the powder led to consumption of local H_2 and prevented the test wire potential from decreasing further until the surface of the powder was completely reduced. XPS of the Pd powder prior to the

reaction confirmed that an oxide layer was present before the ALED process, but not after (Figure S2 in Supporting Information). This suggests that, through intermittent contact between PdO on the surface of the powder and the wire, and by their effects on the solution composition, an equilibrium between the PdO on the powder particles and the wire was reached. These results underscore the need for effective stirring to ensure potential equilibrium between the Pd wire and the Pd particles.

Subsequently, the cell voltage dropped, and a plateau was observed near -0.2 V (region C, Figure 2), which is the expected value for a Pd hydride electrode. At this point, the reagent gas bubbling was terminated (region D, Figure 2). The H_2 partial pressure used is insufficient to cause PdH_α to convert to PdH_β at room temperature.⁴⁸ At this stage of the reaction, hydrogen would be present in the system only as a surface hydride and as dilute PdH_α in the bulk. The small amount of H_2 dissolved in the electrolyte under static pressure is insufficient to reduce the metal salt, as shown in separate control experiments (Figures S3 and S4 in the Supporting Information). Exposing 0.1 M H_2SO_4 to 1% H_2/N_2 gas in the absence of Pd powder, followed by addition of $RhCl_3$ or $(NH_4)_2(PtCl_4)$, showed no decrease in metal salt concentration on the time scale of the deposition cycles described below.

Sequential additions of small aliquots of $RhCl_3$ without gas bubbling are marked in region E of Figure 2. With each addition, the OCP increased. This suggests galvanic replacement of PdH at the surface with Rh. After four aliquots totaling 1.4 DU, a larger jump in OCP was observed, suggesting residual Rh^{III} was present in solution (the formal potential of the $Rh/RhCl_6^{3-}$ redox couple is 0.23 V). A 300 mV increase was observed upon a subsequent addition of $RhCl_3$, suggesting that all hydride present in the system had been consumed. The slight downward drift of the potential after each aliquot was likely due to transport of H_2 from the headspace into the solution and reduction of excess Rh^{III} , but this process was slow compared to the potential jumps corresponding to each dose. Charging the Pd powder with H_2 a second time (region F, Figure 2) by again bubbling the 1% H_2/N_2 gas into the suspension, gave rise to a decrease in OCP to about -0.2 V. The gas bubbling was then stopped (region G, Figure 2). Small increases in OCP were observed as each of several aliquots of $RhCl_3$ was added (region H, Figure 2), with the largest increase observed after the fifth aliquot, corresponding to a cumulative dose of 1.3 DU. An increase in OCP of ~ 300 mV was observed upon subsequent addition, similarly to the first cycle. The Pd wire, acting as a probe of the potential of the Pd powder in suspension, suggests that PdH reducing equivalents sufficient to reduce between 1 and 2 DU of metal salt were formed while charging the cell with the dilute H_2 gas. This could be repeated by forming surface hydrides with either the Rh overlayer or with exposed Pd and by forming dilute PdH_α as previously described. Polycrystalline films,⁴⁹ single crystals,⁵⁰ and NP⁵¹ of Rh have all been demonstrated to adsorb hydrogen, with a coverage of 1.68 reported at 298 K and 1.2 Pa in the first case.⁵¹ Furthermore, it seems reasonable to expect that near its surface, Pd with one to a few monolayers of Rh deposited would exhibit properties similar to PdRh alloys, which absorb hydrogen at much lower pressure than pure Rh.

XPS Characterization of Surface-Modified Powders. XPS spectra of PdRh and PdPt samples that were prepared by addition of varying amounts of metal salt to Pd powder substrates are shown in Figure 3. Deposits formed with a single-

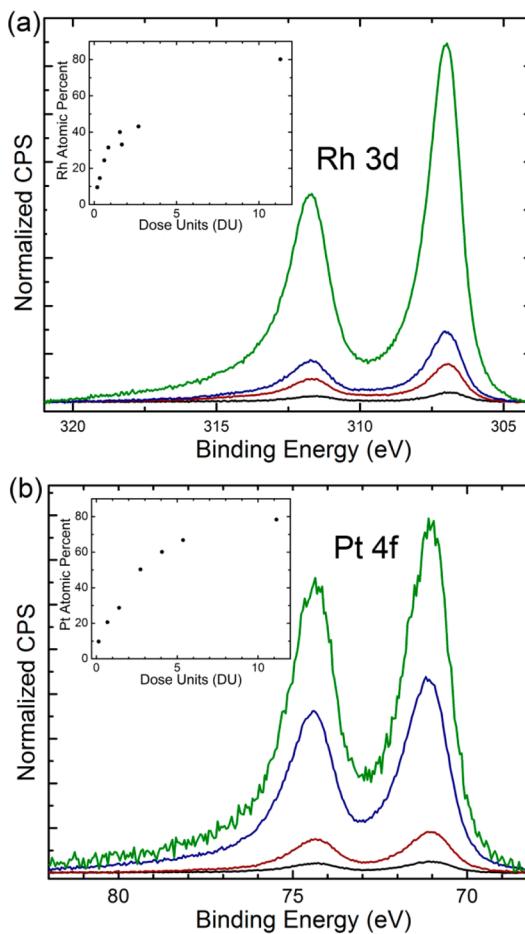


Figure 3. XPS spectra showing the PdRh 3d region (a) and the PdPt 4f region (b) with varying deposit thickness. The Pd 3d peaks in parts a and b for samples with varying deposit thickness were normalized. Samples shown are submonolayer deposition (black), and after one (red), four (blue), and eight (green) cycles of ALED. Insets show XPS quantitation of atomic percent Rh (a) and Pt (b) relative to Pd. Incident photon energy was 1490 eV.

cycle deposition of <1 DU and multiple cycles of deposition are shown. Doses below 2 DU were added in a single aliquot, and those above 2 DU were added in cycles of hydride formation, followed by addition of between 0.9 and 1.8 DU (Table S1 in Supporting Information). As shown in the insets of Figure 3, a more rapid increase in the atomic percent of the adlayer metal was observed at lower cumulative dose for both PdRh and PdPt. This was expected in a regime where not all of the reductant has been consumed and the metal salt is the limiting reagent. The decreased rate of increase for deposits formed from multiple cycles may be due to the diminished driving force for surface hydride formation once a Rh overlayer has formed. The resulting decrease in hydrogen to metal stoichiometry would lead to less deposition per cycle.

ALED on Carbon-Supported Pd Catalyst. The PdRh and PdPt samples discussed above were prepared using Pd powders as substrates, having particle sizes from hundreds of nanometers to a few micrometers. To demonstrate the suitability of this method for deposition of an adlayer metal on high-surface-area substrates, ALED was carried out on commercially available 10% Pd/C (Pd NP suspended on finely divided carbon). This material is an important catalyst for chemical reactions, including hydrogenation and carbon–carbon coupling.^{52,53}

Further, metal NPs supported on carbon are viewed as critical catalysts for emerging, renewable energy technologies, such as hydrogen evolution in solar-to-fuel processes,⁵⁴ and oxygen reduction in proton exchange membrane fuel cells.⁵⁵ The ability to modify the surfaces of such materials in a scalable and cost-effective manner is an important advantage of the ALED process described herein. XPS spectra before and after one cycle of ALED of Rh on Pd/C (420 mmol Rh³⁺/mol Pd) (Figure 4) confirm successful deposition. Compared with the

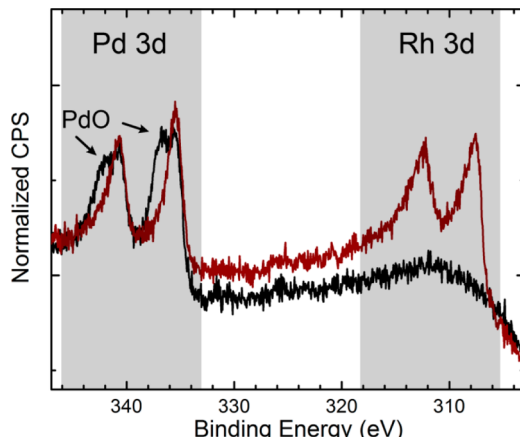


Figure 4. XPS spectra of Pd/C and PdRh/C before (black) and after (red) ALED. Incident photon energy was 1490 eV.

Pd powders, in this case, a much larger dose of metal salt was used during the deposition step due to the larger surface area. Similar to observations of the coarser, unsupported powder substrate, a substantial PdO peak at a binding energy 2–3 eV higher than the Pd 3d peak was present in the spectrum of the Pd/C substrate and absent in that of the PdRh sample after deposition (Figure 4).

Characterization of the Deposited Overlayer of PdRh by STEM and ERXPS. High-resolution STEM images of sectioned PdRh prepared by two cycles of ALED and their corresponding EDS spectral images are shown in Figure 5. The spectra provide direct evidence of the morphology of the overlayer. A thin, conformal layer of Rh is apparent from the elemental maps in Figure 5c,f on two particles at different magnification. This overlayer does not appear to exceed 2 nm in thickness at the particles' surfaces, although geometric effects from the fact that this is a thin section from a more complicated 3D structure could cause the appearance of thickness variations in projection that are not representative of the actual sample morphology. These data argue strongly against extended regions of 3D growth (forming dendrites or Rh particle outgrowths), as has been observed when the adlayer metal was deposited on Pd that was saturated with hydrogen (PdH _{β}).³² A line scan showing the Rh atomic fraction across 25 nm (Figure 6) graphically demonstrates that the Rh-enriched surface observed has a maximum thickness of ~2 nm. The Pd–Rh map in Figure 6 also suggests that the Rh overlayer is somewhat thinner in some regions, and there may be gaps or pinholes in the layer exposing bare Pd. No anisotropy in layer thickness is observed that can be correlated with the direction of sectioning, so it is unlikely that the sectioning process has affected the layer. Figures 5 and 6 also show that Rh was effectively deposited, even on recessed areas of the surface of the particle having subnanometer dimensions. This demonstrates that the

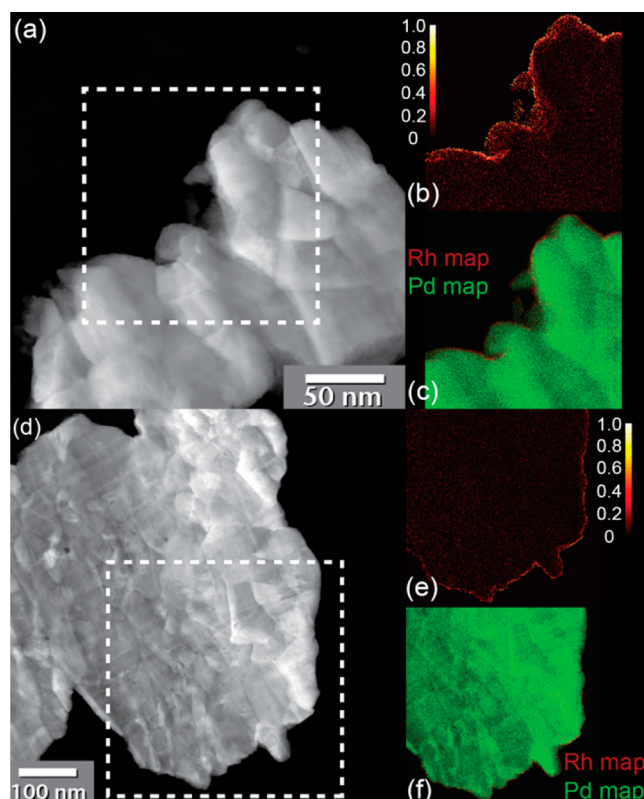


Figure 5. STEM images of PdRh ((a) and (d)) with corresponding Rh atomic fraction ((b) and (e)) and Pd and Rh maps ((c) and (f)) from STEM-EDS measurements.

present method is suitable for uniform deposition of an adlayer of different metals while preserving finely nanostructured geometries.

XPS of the Rh layer formed on PdRh during ALED was carried out with variable-energy photons from a synchrotron source, along with a conventional Al K α X-ray source.³⁸ XPS provided quantitative information on the surface elemental composition, sampling micrometer-scale areas, as opposed to the nanometer scale resolution achieved using the electron microscope. Varying the energy of the incident X-ray photons allowed variation of the mean free paths of the photoelectrons. Spectra at each of the photon energies were, in effect, sampling a different depth. This approach, known as energy-resolved XPS (ERXPS), allows construction of a “depth profile” for the nanostructured materials.^{56–58} ERXPS has been demonstrated to be more effective than other techniques in establishing depth profiles of powders and samples with high surface roughness.^{58,59}

XPS spectra of PdRh after two cycles of ALED were collected at three photon energies (Figure 7a). The signal of Rh increased relative to that of Pd as the sample was probed with photons of decreasing energy, demonstrating enrichment in Rh at the surface. This can be seen quantitatively in the inset of Figure 7a, where the ratio of XPS signal intensities for Rh compared with Pd increases from 0.6 to 3 moving from photons of 1490 eV (Al K α) to 450 eV.

Because the 3d electrons of Pd and Rh have different (albeit similar) binding energies, analysis of the depth profile is complicated by differences in photoelectron mean free paths. The depth profile is further obscured when some degree of three-dimensional growth is considered. To address these

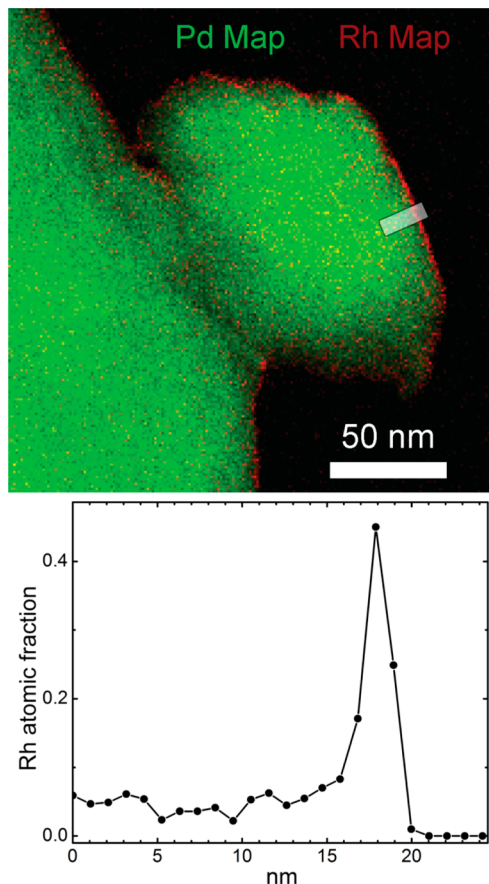


Figure 6. Pd and Rh maps for PdRh with two cycles of deposition (top) and a line scan showing the change in Rh atomic fraction across 25 nm, originating within the particle and extending across the surface.

concerns, the software package SESSA was used to simulate XPS spectra with X-ray photons of 450, 850, and 1490 eV for a Rh film on a Pd substrate.³⁹ Satisfactory agreement with experimental data at all three energies, however, was not obtained by simply changing the thickness of the Rh film. To consider a three-dimensional growth model, a basis set of simulated spectra was constructed at each photon energy comprising (i) bare Pd, (ii) PdRh having a Rh thickness of 4 Å, and (iii) PdRh having a Rh thickness of 8 Å. The three spectra at each photon energy were combined to simulate a Rh layer of varied thickness. Root mean squared errors (RMSE) between the simulated and actual spectra for several combinations of fractional coverage are shown in Table 1. The lowest values of RMSE were obtained for combinations with 70–80% Rh coverage, the majority of which was 8 Å in thickness, with a small or no contribution from a 4 Å layer. The best fit was obtained with a surface comprising 76% 8 Å Rh coverage with 24% bare Pd (Figure 7b). For satisfactory agreement with experimental spectra, it was necessary that the model include a substantial fraction of bare Pd. These data suggest that growth during each cycle was not strictly confined to a single atomic layer, and a second layer was forming before completion of the first. The galvanic exchange reaction was not perfectly local, though it has been shown to be nearly so in studies of SLRR of underpotentially deposited layers.^{27,28,60}

Electrochemical Hydrogen Absorption and Desorption on Surface-Modified Pd. Inspection of the CV of the Pd powders after ALED and the rate of hydrogen desorption

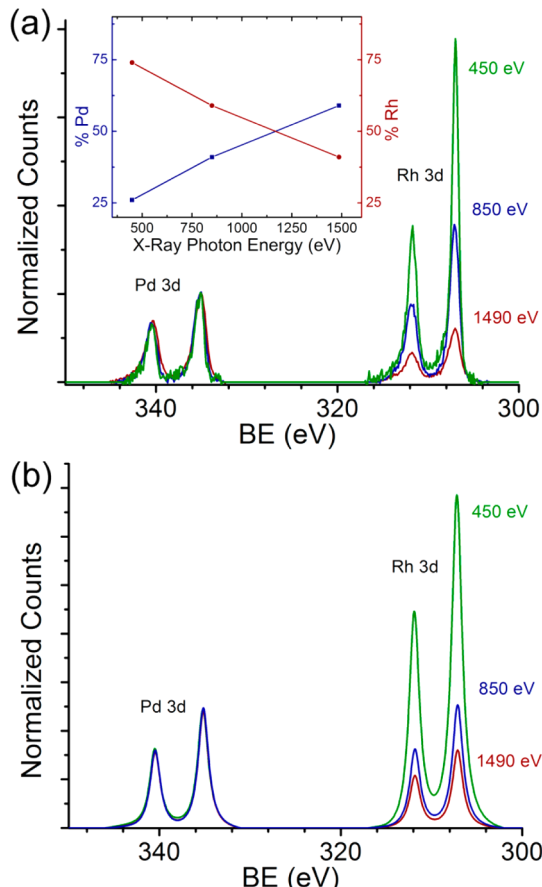


Figure 7. XPS spectra collected at three different photon energies (a) and simulated spectra based on a three-layer growth model (b). Inset shows depth profile, or the atomic percent Pd and Rh at the photoelectron mean free path corresponding to each element, at each photon energy.

Table 1. RMS Error in Rh Atom Percent between XPS Spectra Collected with 450, 850, and 1490 eV Photons and Spectra Simulated Using SESSA at Those Three Energies^a

Pd	4 Å layer	8 Å layer	RMSE
0.24		0.76	3.6
0.23	0.05	0.72	3.8
0.23	0.07	0.70	4.0
0.21	0.14	0.65	4.3
0.14	0.46	0.40	6.7
0.05	0.95		11.4
	1.00		11.8
		1.00	19.4

^aThese data are obtained using background-corrected spectra of PdRh with two cycles of deposition. Atom percent is calculated using the integrated area under the Pd and Rh 3d peaks.

indicate a change in surface states (Figure 8). When the potential was scanned negative to −0.4 V, reduction currents were observed, which is indicative of the formation of adsorbed, absorbed, and molecular hydrogen (Figure 8, insets). During the return scan to 0.35 V, corresponding oxidative currents from hydrogen desorption were observed. In the case of both PdRh and PdPt, the onset of the oxidative features occurred at more negative potential than was observed for the PdPd (1.8 DU) control sample, suggesting increased kinetics of hydrogen desorption. A small effect was seen with the thinnest PdRh

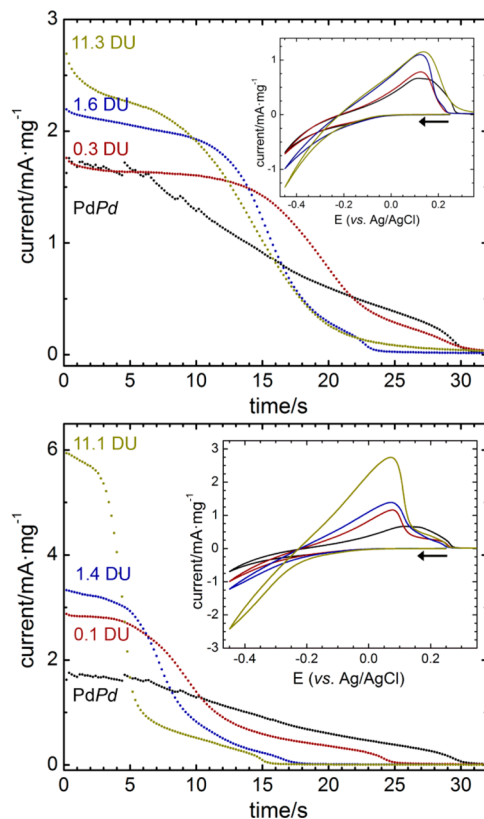


Figure 8. Current from desorption of hydrogen from PdRh (top) and PdPt (bottom) compared with PdPd. PdRh samples have DUs of 0.3 (red), 1.6 (blue), and 11.3 (8 cycles, green). PdPt samples have DU of 0.1 (red), 1.4 (blue), and 11.1 (8 cycles, green). The same PdPd sample (1.8 DU) is shown in black on both plots. Powders were first charged with hydrogen by applying 1.5 mA of current for 60 s. Subsequently, they were held at 0.27 V vs Ag/AgCl, and desorption current measured vs time. Input charge (90 mC) is conserved to $\geq 97\%$ during desorption. Inset shows CV, beginning with a negative scan from 0.35 to -0.45 V, cycling back to 0.35 V, at 150 mV/s, in 0.1 M H_2SO_4 (cycle 20).

overlayer (0.3 DU), which increased with larger doses (1.6 DU and 11.3 DU, one and eight cycles, respectively). The effect was also observed for PdPt samples, to an even greater extent, and the onset potential shifted progressively more negative in samples prepared with 0.1, 1.4, and 11.1 DU.

The increased rate of hydrogen desorption can be seen more quantitatively by monitoring the decay in the current while holding the potential at 0.27 V after applying a current of 1.5 mA for 60 s to load the sample with hydrogen (Figure 8). In those experiments, the charge from desorption was conserved to $>97\%$ of that measured during the hydrogen-loading phase. As the CV data suggest, the initial current was higher for samples of PdRh and PdPt compared with PdPd, and the effect was more pronounced with larger doses. The kinetic improvements suggested by these data for surface-modified Pd are generally consistent with observations reported for Rh-modified Pd nanofilms grown using SLRR³⁶ and nanostructured Pd with adsorbates or submonolayer Pt deposits.¹³ Modification of surface hydride energetics resulting from the Rh or Pt overlayers is a likely explanation for this behavior, given the similarity between the PdPd control and the PdRh and PdPt samples, which differed only in the identity of the adlayer metal used during ALED.

CONCLUSIONS

In the atomic-layer electroless deposition (ALED) process, electroless (chemical) formation of surface PdH and dilute PdH_a is followed by galvanic replacement with a metal salt on the substrate surface. The electrolyte is optionally replaced to remove excess metal salt, although that was not demonstrated here. To grow thicker films, these two or three steps are repeated. High-resolution STEM-EDS measurements indicate that a conformal deposit is formed during this process. ERXPS measurements of PdRh formed using two cycles of ALED agree with a simulated growth model with 70–80% of the surface covered with Rh. XPS data also showed that the thickness of the coating increased as additional ALED cycles were performed. CV data suggested that the overlayers of Rh and Pt improve the kinetics of hydrogen reduction and oxidation.

Several advantages could be realized with this approach. The process is scalable, even on high surface area materials in which high electrode currents would present complications for an electrodeposition process. Further, nanoscale features, such as nanopores, should not be perturbed under the low-temperature conditions used during processing. The extent to which the solution-phase reagents implemented here can penetrate deeply into high-aspect-ratio features is worthy of future investigations. STEM-EDS spectral maps demonstrated that uniform coverage occurred even on narrow cavities and protrusions with subnanometer dimensions, suggesting that this method is amenable to substrates having irregular surfaces or complex three-dimensional features. Furthermore, this method can be used to modify the surface of commercially available Pd/C, a material routinely used for chemical catalysis. Since no specialized equipment is required, this technique could be routinely carried out by synthetic chemists to make use of enhanced properties of surface-modified catalysts. This method is a general, scalable, and mild strategy for deposition of atomic-scale layers of metals on a variety of substrates.

ASSOCIATED CONTENT

Supporting Information

A schematic of the cell used for synthesis of surface-modified powders (Figure S1), XPS spectra of Pd substrate powder before and after one cycle (Figure S2), ultraviolet-visible spectra of metal salt solutions in the presence of hydrogen (Figures S3 and S4), and the data corresponding to Figure 3 (Table S1) are available free of charge via the Internet at <http://pubs.acs.org>.

AUTHOR INFORMATION

Corresponding Author

*Address: Sandia National Laboratories, PO Box 969, Mail Stop 9292, Livermore, CA, USA. Phone: 925-294-6613. E-mail: drobins@sandia.gov.

Author Contributions

The manuscript was written through contributions of all authors. All authors have given approval to the final version of the manuscript.

Notes

The authors declare no competing financial interest.

ACKNOWLEDGMENTS

Sandia National Laboratories is a multiprogram laboratory managed and operated by Sandia Corporation, a wholly owned subsidiary of Lockheed Martin Corporation, for the U.S.

Department of Energy's National Nuclear Security Administration under contract DE-AC04-94AL85000. The Advanced Light Source is supported by the Director, Office of Science, Office of Basic Energy Sciences, of the U.S. Department of Energy under Contract No. DE-AC02-05CH11231. Support for J.L.S. was in part provided by the National Science Foundation, Division of Materials Research, Grant No. 1006747. The authors also thank Mark Homer for STEM sample preparation and David M. Benson for his comments during manuscript preparation.

■ REFERENCES

- (1) Liu, N.; Tang, M. L.; Hentschel, M.; Giessen, H.; Alivisatos, A. P. Nanoantenna-enhanced gas sensing in a single tailored nanofocus. *Nat. Mater.* **2011**, *10* (8), 631–636.
- (2) Avila, J. I.; Matelon, R. J.; Trabol, R.; Favre, M.; Lederman, D.; Volkmann, U. G.; Cabrera, A. L. Optical properties of Pd thin films exposed to hydrogen studied by transmittance and reflectance spectroscopy. *J. Appl. Phys.* **2010**, *107* (2), 023504-1–023504-4.
- (3) Li, M.; Yang, W. F. Highly porous palladium bulk: Preparation and properties as active metal material for displacement chromatographic process. *Int. J. Hydrogen Energy* **2009**, *34* (3), 1585–1589.
- (4) Burwell, R. Supported platinum, palladium, and rhodium catalysts. *Langmuir* **1986**, *2* (1), 2–11.
- (5) Astruc, D.; Lu, F.; Aranzaes, J. R. Nanoparticles as recyclable catalysts: The frontier between homogeneous and heterogeneous catalysis. *Angew. Chem., Int. Ed.* **2005**, *44* (48), 7852–7872.
- (6) Dominguez-Dominguez, S.; Berenguer-Murcia, A.; Pradhan, B. K.; Linares-Solano, A.; Cazorla-Amoros, D. Semihydrogenation of phenylacetylene catalyzed by palladium nanoparticles supported on carbon materials. *J. Phys. Chem. C* **2008**, *112* (10), 3827–3834.
- (7) Shao, M. Palladium-based electrocatalysts for hydrogen oxidation and oxygen reduction reactions. *J. Power Sources* **2011**, *196* (5), 2433–2444.
- (8) Bianchini, C.; Shen, P. K. Palladium-based electrocatalysts for alcohol oxidation in half cells and in direct alcohol fuel cells. *Chem. Rev.* **2009**, *109* (9), 4183–4206.
- (9) Zhang, J. T.; Qiu, C. C.; Ma, H. Y.; Liu, X. Y. Facile fabrication and unexpected electrocatalytic activity of palladium thin films with hierarchical architectures. *J. Phys. Chem. C* **2008**, *112* (36), 13970–13975.
- (10) Vidal-Iglesias, F. J.; Solla-Gullón, J.; Herrero, E.; Aldaz, A.; Feliu, J. M. Pd adatom decorated (100) preferentially oriented Pt nanoparticles for formic acid electrooxidation. *Angew. Chem., Int. Ed.* **2010**, *49* (39), 6998–7001.
- (11) Chen, J. G.; Menning, C. A.; Zellner, M. B. Monolayer bimetallic surfaces: Experimental and theoretical studies of trends in electronic and chemical properties. *Surf. Sci. Rep.* **2008**, *63* (5), 201–254.
- (12) Greeley, J.; Mavrikakis, M. Surface and subsurface hydrogen: Adsorption properties on transition metals and near-surface alloys. *J. Phys. Chem. B* **2005**, *109* (8), 3460–3471.
- (13) Bartlett, P. N.; Marwan, J. The effect of surface species on the rate of H sorption into nanostructured Pd. *Phys. Chem. Chem. Phys.* **2004**, *6* (11), 2895–2898.
- (14) Lee, H.; Habas, S. E.; Somorjai, G. A.; Yang, P. Localized Pd overgrowth on cubic Pt nanocrystals for enhanced electrocatalytic oxidation of formic acid. *J. Am. Chem. Soc.* **2008**, *130* (16), 5406–5407.
- (15) Llorca, M. J.; Feliu, J. M.; Aldaz, A.; Clavilier, J. Formic acid oxidation on $Pd_{ad} + Pt(100)$ and $Pd_{ad} + Pt(111)$ electrodes. *J. Electroanal. Chem.* **1994**, *376* (1–2), 151–160.
- (16) Stamenkovic, V. R.; Mun, B. S.; Arenz, M.; Mayrhofer, K. J. J.; Lucas, C. A.; Wang, G. F.; Ross, P. N.; Markovic, N. M. Trends in electrocatalysis on extended and nanoscale Pt-bimetallic alloy surfaces. *Nat. Mater.* **2007**, *6* (3), 241–247.
- (17) Souza-Garcia, J.; Herrero, E.; Feliu, J. Breaking the C–C bond in the ethanol oxidation reaction on platinum electrodes: effect of steps and ruthenium adatoms. *ChemPhysChem* **2010**, *11* (7), 1391–1394.
- (18) Pálánkó, I. Effects of surface modifiers on the liquid-phase hydrogenation of alkenes over silica-supported platinum, palladium and rhodium catalysts I. Quinoline and carbon tetrachloride. *Appl. Catal., A* **1995**, *126* (1), 39–49.
- (19) George, S. Atomic layer deposition: an overview. *Chem. Rev.* **2010**, *110* (1), 111–31.
- (20) Christensen, S. T.; Elam, J. W. Atomic layer deposition of Ir–Pt alloy films. *Chem. Mater.* **2010**, *22* (8), 2517–2525.
- (21) Mackus, A.; Garcia-Alonso, D.; Knoops, H.; Bol, A.; Kessels, W. Room-temperature atomic layer deposition of platinum. *Chem. Mater.* **2013**, *25* (9), 1769–1774.
- (22) Chang, S. L. Y.; Barnard, A. S.; Dwyer, C.; Hansen, T. W.; Wagner, J. B.; Dunin-Borkowski, R. E.; Weyland, M.; Konishi, H.; Xu, H. Stability of porous platinum nanoparticles: combined *in situ* TEM and theoretical study. *J. Phys. Chem. Lett.* **2012**, *3* (9), 1106–1110.
- (23) Klein, M. P.; Jacobs, B. W.; Ong, M. D.; Fares, S. J.; Robinson, D. B.; Stavila, V.; Wagner, G. J.; Arslan, I. Three-dimensional pore evolution of nanoporous metal particles for energy storage. *J. Am. Chem. Soc.* **2011**, *133* (24), 9144–9147.
- (24) Lei, Y.; Liu, B.; Lu, J.; Lobo-Lapidus, R. J.; Wu, T.; Feng, H.; Xia, X.; Mane, A. U.; Libera, J. A.; Greeley, J. P.; Miller, J. T.; Elam, J. W. Synthesis of Pt–Pd core–shell nanostructures by atomic layer deposition: application in propane oxidative dehydrogenation to propylene. *Chem. Mater.* **2012**, *24* (18), 3525–3533.
- (25) Stickney, J. L., Electrochemical atomic layer epitaxy (EC-ALE): nanoscale control in the electrodeposition of compound semiconductors. In *Advances in Electrochemical Science and Engineering*; Wiley-VCH Verlag GmbH: Weinheim, 2001; Vol. 7; pp 1–105.
- (26) Pathan, H. M.; Lokhande, C. D. Deposition of metal chalcogenide thin films by successive ionic layer adsorption and reaction (SILAR) method. *Bull. Mater. Sci.* **2004**, *27* (2), 85–111.
- (27) Sheridan, L. B.; Youn-Geun, K.; Perdue, B. R.; Jagannathan, K.; Stickney, J. L.; Robinson, D. B. Hydrogen adsorption, absorption, and desorption at palladium nanofilms formed on Au(111) by electrochemical atomic layer deposition (E-ALD): studies using voltammetry and *in situ* scanning tunneling microscopy. *J. Phys. Chem. C* **2013**, *117* (30), 15728–15740.
- (28) Sheridan, L. B.; Gebregziabiher, D. K.; Stickney, J. L.; Robinson, D. B. Formation of palladium nanofilms using electrochemical atomic layer deposition (E-ALD) with chloride complexation. *Langmuir* **2013**, *29* (5), 1592–1600.
- (29) Fayette, M.; Liu, Y.; Bertrand, D.; Nutariya, J.; Vasiljevic, N.; Dimitrov, N. From Au to Pt via surface limited redox replacement of Pb UPD in one-cell configuration. *Langmuir* **2011**, *27* (9), 5650–5658.
- (30) Brankovic, S. R.; Wang, J. X.; Adžić, R. R. Metal monolayer deposition by replacement of metal adlayers on electrode surfaces. *Surf. Sci.* **2001**, *474* (1–3), L173–L179.
- (31) Nutariya, J.; Fayette, M.; Dimitrov, N.; Vasiljevic, N. Growth of Pt by surface limited redox replacement of underpotentially deposited hydrogen. *Electrochim. Acta* **2013**, *112*, 813–823.
- (32) Zolfaghari, A.; Conway, B. E. Electroless deposition of Pt at a Pd electrode by reaction with sorbed H in Pd/H. *J. Electroanal. Chem.* **2000**, *488* (2), 151–153.
- (33) Adžić, R. R.; Wang, J. X. *Hydrogen absorption induced metal deposition on Pd and Pd-alloy Particles*. US Patent No. 7,507,495, 2009.
- (34) Gómez, R.; Rodes, A.; Pérez, J. M.; Feliu, J. M.; Aldaz, A. Electrochemical and *in situ* FTIR studies of the CO adsorption at palladium and rhodium multilayers deposited on platinum single crystal surfaces. I. Pt(110) substrate. *Surf. Sci.* **1995**, *327* (3), 202–215.
- (35) Llorca, M. J.; Feliu, J. M.; Aldaz, A.; Clavilier, J. Electrochemical structure-sensitive behaviour of irreversibly adsorbed palladium on Pt(100), Pt(111) and Pt(110) in an acidic medium. *J. Electroanal. Chem.* **1993**, *351* (1–2), 299–319.
- (36) Sheridan, L. B.; Yates, V. M.; Benson, D. M.; Stickney, J. L.; Robinson, D. B. Hydrogen sorption properties of bare and Rh-

- modified Pd nanofilms grown via surface limited redox replacement reactions. *Electrochim. Acta* **2014**, *128*, 400–405.
- (37) Powell, C. J.; Jablonski, A. *NIST Electron Inelastic-Mean-Free-Path Database Version 1.2, SRD 71*; National Institutes of Standards and Technology: Gaithersburg, MD, 2010.
- (38) Grass, M. E.; Karlsson, P. G.; Aksoy, F.; Lundqvist, M.; Wannberg, B.; Mun, B. S.; Hussain, Z.; Liu, Z. New ambient pressure photoemission endstation at Advanced Light Source beamline 9.3.2. *Rev. Sci. Instrum.* **2010**, *81* (5), 053106-1–053106-7.
- (39) Smekal, W.; Werner, W. S. M.; Powell, C. J. Simulation of electron spectra for surface analysis (SESSA): a novel software tool for quantitative Auger-electron spectroscopy and X-ray photoelectron spectroscopy. *Surf. Interface Anal.* **2005**, *37* (11), 1059–1067.
- (40) Hochella, M. F., Jr.; Moore, J. N.; Golla, U.; Putnis, A. A TEM study of samples from acid mine drainage systems: metal-mineral association with implications for transport. *Geochim. Cosmochim. Acta* **1999**, *63* (19–20), 3395–3406.
- (41) Johnson, P. B.; Thomson, R. W.; Reader, K. TEM and SEM studies of radiation blistering in helium-implanted copper. *J. Nucl. Mater.* **1999**, *273* (2), 117–129.
- (42) Cliff, G.; Lorimer, G. W. The quantitative analysis of thin specimens. *J. Microsc. (Oxford)* **1975**, *103* (2), 203–207.
- (43) Ong, M. D.; Jacobs, B. W.; Sugar, J. D.; Grass, M. E.; Liu, Z.; Buffleben, G. M.; Clift, W. M.; Langham, M. E.; Cappillino, P. J.; Robinson, D. B. Effect of rhodium distribution on thermal stability of nanoporous palladium-rhodium powders. *Chem. Mater.* **2012**, *24* (6), 996–1004.
- (44) Lynch, J. F.; Flanagan, T. B. Investigation of dynamic equilibrium between chemisorbed and absorbed hydrogen in palladium-hydrogen system. *J. Phys. Chem.* **1973**, *77* (22), 2628–2634.
- (45) Simons, J. W.; Flanagan, T. B. Absorption isotherms of hydrogen in alpha-phase of hydrogen-palladium system. *J. Phys. Chem.* **1965**, *69* (11), 3773–3781.
- (46) Lewis, F. A. *The Palladium Hydrogen System*. Academic Press: New York, NY, 1967; p 178.
- (47) Ruetschi, P.; Amilie, R. F. Solubility of hydrogen in potassium hydroxide and sulfuric acid. Salting-out and hydration. *J. Phys. Chem.* **1966**, *70* (3), 718–723.
- (48) Lässer, R.; Klatt, K. H. Solubility of hydrogen isotopes in palladium. *Phys. Rev. B* **1983**, *28* (2), 748–758.
- (49) Duś, R.; Nowicka, E.; Nowakowski, R. Hydrogen adsorption on rhodium: Hydride formed on the surface of thin rhodium films. *Appl. Surf. Sci.* **2008**, *254* (14), 4286–4291.
- (50) Castner, D. G.; Sexton, B. A.; Somorjai, G. A. Leed and thermal desorption studies of small molecules (H_2 , O_2 , CO, CO_2 , NO, C_2H_4 , C_2H_2 and C) chemisorbed on the rhodium (111) and (100) surfaces. *Surf. Sci.* **1978**, *71* (3), 519–540.
- (51) Kobayashi, H.; Morita, H.; Yamauchi, M.; Ikeda, R.; Kitagawa, H.; Kubota, Y.; Kato, K.; Takata, M. Nanosize-induced hydrogen storage and capacity control in a non-hydride-forming element: rhodium. *J. Am. Chem. Soc.* **2011**, *133* (29), 11034–11037.
- (52) Crespo-Quesada, M.; Cárdenas-Lizana, F.; Dessimoz, A.-L.; Kiwi-Minsker, L. Modern trends in catalyst and process design for alkyne hydrogenations. *ACS Catal.* **2012**, *2* (8), 1773–1786.
- (53) Yin, L.; Liebscher, J. carbon–carbon coupling reactions catalyzed by heterogeneous palladium catalysts. *Chem. Rev.* **2007**, *107* (1), 133–173.
- (54) Dasgupta, N. P.; Liu, C.; Andrews, S.; Prinz, F. B.; Yang, P. Atomic layer deposition of platinum catalysts on nanowire surfaces for photoelectrochemical water reduction. *J. Am. Chem. Soc.* **2013**, *135* (35), 12932–12935.
- (55) Wu, J.; Yang, H. Platinum-based oxygen reduction electrocatalysts. *Acc. Chem. Res.* **2013**, *46* (8), 1848–1857.
- (56) Tao, F.; Grass, M. E.; Zhang, Y.; Butcher, D. R.; Renzas, J. R.; Liu, Z.; Chung, J. Y.; Mun, B. S.; Salmeron, M.; Somorjai, G. A. Reaction-driven restructuring of Rh-Pd and Pt-Pd core–shell nanoparticles. *Science* **2008**, *322* (5903), 932–934.
- (57) Tao, F.; Grass, M. E.; Zhang, Y.; Butcher, D. R.; Aksoy, F.; Aloni, S.; Altoe, V.; Alayoglu, S.; Renzas, J. R.; Tsung, C.-K.; Zhu, Z.; Liu, Z.; Salmeron, M.; Somorjai, G. A. Evolution of structure and chemistry of bimetallic nanoparticle catalysts under reaction conditions. *J. Am. Chem. Soc.* **2010**, *132* (25), 8697–8703.
- (58) Haverkamp, R. G.; Marshall, A. T.; Cowie, B. C. C. Energy resolved XPS depth profile of (IrO_2 , RuO_2 , Sb_2O_5 , SnO_2) electrocatalyst powder to reveal core–shell nanoparticle structure. *Surf. Interface Anal.* **2011**, *43* (5), 847–855.
- (59) Merzlikin, S. V.; Tolkachev, N. N.; Strunskus, T.; Witte, G.; Glogowski, T.; Wöll, C.; Grünert, W. Resolving the depth coordinate in photoelectron spectroscopy – Comparison of excitation energy variation vs. angular-resolved XPS for the analysis of a self-assembled monolayer model system. *Surf. Sci.* **2008**, *602* (3), 755–767.
- (60) Sheridan, L.; Czerwinski, J.; Jayaraju, N.; Gebregziabiher, D.; Stickney, J.; Robinson, D.; Soriaga, M. Electrochemical atomic layer deposition (E-ALD) of palladium nanofilms by surface limited redox replacement (SLRR), with EDTA complexation. *Electrocatal.* **2012**, *3* (2), 96–107.